2019

First Approach to Coupling of Numerical Lifting-Line Theory and Linear Covariance Analysis for UAV State Uncertainty Propagation

Cory D. Goates
Utah State University

Randall S. Christensen
Utah State University

Robert Leishman
Air Force Institute of Technology

First Approach to Coupling of Numerical Lifting-Line Theory and Linear Covariance Analysis for UAV State Uncertainty Propagation

Cory D. Goates * and Randall S. Christensen †
Utah State University, Logan, Utah, 84322-4130

Numerical lifting-line is a computationally efficient method for calculating aerodynamic forces and moments on aircraft. However, its potential has yet to be tapped for use in guidance, navigation, and control (GN&C). Linear covariance analysis is becoming a popular GN&C design tool and shows promise for pairing with numerical lifting-line. Pairing numerical lifting-line with linear covariance analysis allows for forward propagation of state uncertainty for real-time decision making. We demonstrate this for select state variables in a drone aerial recapture situation. Linear covariance analysis uses finite difference derivatives obtained from numerical lifting-line to calculate force and moment variances. These show agreement with Monte Carlo simulation results to within 10%, without the significant computational cost of Monte Carlo. These results show numerical lifting-line can be used in linear covariance analysis of an entire UAV GN&C solution. Not only does this allow for real-time uncertainty propagation, but also faster and more thorough multi-disciplinary design optimization.

Nomenclature

α = aerodynamic angle of attack

α_0 = lifting surface mounting angle

b = span

β = aerodynamic sideslip angle

c = chord length

$\bar{c}$ = mean aerodynamic chord length

$\tilde{C}_L$ = section lift coefficient

$\tilde{C}_m$ = section moment coefficient

δ = flap or control deflection

$\boldsymbol{f}$ = aerodynamic force vector

*Graduate Research Assistant. Mechanical & Aerospace Engineering Department. 4130 Old Main Hill.
†Assistant Professor. Electrical & Computer Engineering Department. 4130 Old Main Hill.

G = dimensionless vortex strength

Γ = vortex strength

$[\boldsymbol{J}]$ = aircraft inertia tensor

l = length

L = lift force

Λ = sweep angle

$\boldsymbol{m}$ = aerodynamic moment vector

M = number of Monte Carlo simulation samples

N = number of horseshoe vortices/control points

$\boldsymbol{\omega}$ = aircraft angular rate vector

$\boldsymbol{p}$ = aircraft position vector

$[\boldsymbol{P}]$ = covariance matrix

ϕ = bank angle about the wind x-axis

$\boldsymbol{q}$ = aircraft orientation vector

r = displacement

R_T = lifting surface taper ratio

ρ = density

s = spanwise position

S = planform area

θ = elevation angle about the wind y-axis

$\boldsymbol{u_a}$ = axial direction unit vector

$\boldsymbol{u_n}$ = normal direction unit vector

$\boldsymbol{u}$ = control inputs

v = dimensionless velocity

V = velocity

W = weight

x = x-coordinate

$\boldsymbol{x}$ = aircraft state

y = y-coordinate

z = z-coordinate

ζ = dimensionless length

Subscripts

a = aileron

b = aircraft body frame

e = elevator

h = horizontal stabilizer

i = control point/horseshoe vortex index

ind = induced

∞ = freestream

j = horseshoe vortex index

r = rudder

ref = global reference

s = spanwise direction

v = vertical stabilizer

w = wind frame

w = main wing

0 = inbound horseshoe vortex node

1 = outbound horseshoe vortex node

Superscripts

$\bar{}$ = reference state or trajectory

(Note: Except for covariance matrices, a matrix with a subscript indicates a Jacobian of partial derivatives with respect to the subscript variable vector.)

I. Introduction

LINEAR covariance analysis is an efficient tool for propagating covariances through updates to a system's state. Linear covariance is becoming popular for design and analysis of control systems for unmanned vehicles [1–6]. Traditionally, propagation of uncertainties through complex systems has been accomplished using Monte Carlo simulation, as in [7, 8]. However, Monte Carlo is computationally expensive as hundreds of simulations must be run, which severely limits the breadth of design analysis that can be accomplished [1]. Linear covariance requires only a handful of matrix computations and so allows for trade studies to be run faster and over a much larger portion of the design space. Linear covariance can also be used for real-time uncertainty propagation and decision making in unmanned vehicles. Examples can be found in the literature of using Monte Carlo simulations for real time decision making, as in [9], but this is again computationally expensive. This cannot feasibly be done in real time onboard a UAV with a high level of confidence, whereas linear covariance analysis can.

Linear covariance requires the outputs of each portion of the system model be linearized with respect to inputs. The linearization of navigation and control algorithms for unmanned vehicles is well documented in the literature(for example, see [1, 5]). However, for fixed-wing unmanned aerial vehicles, the vehicle dynamics model, has yet to be linearized based off of rigorous, analytical methods and applied to linear covariance analysis.

Multiple methods exist for modelling the state of an aircraft, such as lifting-line methods, panel methods, and CFD. For fixed-wing aircraft, the most computationally efficient of these methods is numerical lifting-line [10, 11]. Numerical lifting-line is an adaptation of Prandtl's classic lifting-line theory that can model interactions between multiple lifting surfaces. Numerical lifting-line is orders of magnitude faster than panel methods and CFD but is as accurate as CFD for wings with an aspect ratio greater than about four [10, 11]. This makes numerical lifting-line an ideal candidate for the vehicle dynamics model for linear covariance analysis.

One potential application of this pairing is modelling an aerial drone recapture situation. Other attempts have been made in the literature, as in [12], to determine the probability of an automatically controlled airplane achieving a desired trajectory; however, these do not utilize an analytical model of aerodynamics nor do they attempt to investigate the case of multiple interacting flow fields. In such a situation, one has a relatively small aircraft entering the flow field of a much larger aircraft. The larger, leading aircraft introduces large variations in the freestream velocity encountered by the tailing aircraft. Linear covariance analysis can be used by the tailing aircraft's autopilot to propagate uncertainty in its state forward in time to decide whether a recapture is feasible. Numerical lifting-line can provide the sensitivities of aerodynamic forces and moments with respect to the tailing aircraft's state within the flow field which are required for linear covariance analysis.

In this study, we investigate the how effectively linear covariance analysis can predict force and moment covariances for a tailing aircraft at a given position. We present a short derivation of linear covariance analysis and numerical lifting-line theory. We describe how the sensitivity matrices necessary for linear covariance analysis are obtained from numerical lifting-line. We show that the solutions from numerical lifting-line for forces and moments, as well as numerical derivatives, converge with respect to grid size. We then compare the covariances obtained from linear covariance to those determined by Monte Carlo simulation.

II. Linear Covariance Analysis

We here present a shortened derivation of linear covariance analysis (see [13] for the full derivation). Ignoring freestream variations, the motion of a UAV is a nonlinear function of state and control inputs:

$$\dot{\boldsymbol{x}} = f(\boldsymbol{x}, \boldsymbol{u}) \tag{1}$$

Where $\boldsymbol{x}$ is the aircraft state vector:

$$\boldsymbol{x} = \begin{bmatrix} \boldsymbol{p_b} \\ \boldsymbol{V_b} \\ \boldsymbol{q_b} \\ \boldsymbol{\omega_b} \end{bmatrix} \tag{2}$$

And $\boldsymbol{u}$ is the vector of control inputs:

$$\boldsymbol{u} = \begin{bmatrix} \delta_a \\ \delta_e \\ \delta_r \end{bmatrix} \tag{3}$$

From a knowledge of rigid body dynamics, eq. (1) is fully expressed as:

$$\begin{bmatrix} \dot{\boldsymbol{p_b}} \\ \dot{\boldsymbol{V_b}} \\ \dot{\boldsymbol{q_b}} \\ \dot{\boldsymbol{\omega_b}} \end{bmatrix} = \begin{bmatrix} \boldsymbol{V_b} \\ -\boldsymbol{\omega_b} \times \boldsymbol{V_b} + \frac{\boldsymbol{f_b}}{m} \\ \frac{1}{2} \begin{bmatrix} 0 \\ \boldsymbol{\omega_b} \end{bmatrix} \otimes \boldsymbol{q_b} \\ [\boldsymbol{J}]^{-1} \left[-\boldsymbol{\omega_b} \times ([\boldsymbol{J}]\boldsymbol{\omega_b}) + \boldsymbol{m_b} \right] \end{bmatrix} \tag{4}$$

Where the aerodynamic forces and moments are derived from the truth model as a function of aircraft state and control inputs:

$$\boldsymbol{f_b} = Q(\boldsymbol{x}, \boldsymbol{u}) \tag{5}$$

$$\boldsymbol{m_b} = R(\boldsymbol{x}, \boldsymbol{u}) \tag{6}$$

Equation (4) can be linearized about a given reference state or trajectory, $\bar{\boldsymbol{x}}$ and $\bar{\boldsymbol{u}}$, to yield:

$$d\dot{\boldsymbol{x}} = [\boldsymbol{F}]_{\boldsymbol{x}} d\boldsymbol{x} + [\boldsymbol{F}]_{\boldsymbol{Q}} ([\boldsymbol{Q}]_{\boldsymbol{x}} d\boldsymbol{x} + [\boldsymbol{Q}]_{\boldsymbol{u}} d\boldsymbol{u}) + [\boldsymbol{F}]_{\boldsymbol{R}} ([\boldsymbol{R}]_{\boldsymbol{x}} d\boldsymbol{x} + [\boldsymbol{R}]_{\boldsymbol{u}} d\boldsymbol{u}) \tag{7}$$

Where:

$$d\boldsymbol{x} = \boldsymbol{x} - \bar{\boldsymbol{x}} \tag{8}$$

$$\boldsymbol{du} = \boldsymbol{u} - \bar{\boldsymbol{u}} \tag{9}$$

$$[\boldsymbol{Q}]_{\boldsymbol{x}} \equiv \left.\frac{\partial \boldsymbol{f}}{\partial \boldsymbol{x}}\right|_{\boldsymbol{x}=\bar{\boldsymbol{x}},\boldsymbol{u}=\bar{\boldsymbol{u}}} \tag{10}$$

$$[\boldsymbol{Q}]_{\boldsymbol{u}} \equiv \left.\frac{\partial \boldsymbol{f}}{\partial \boldsymbol{u}}\right|_{\boldsymbol{x}=\bar{\boldsymbol{x}},\boldsymbol{u}=\bar{\boldsymbol{u}}} \tag{11}$$

$$[\boldsymbol{R}]_{\boldsymbol{x}} \equiv \left.\frac{\partial \boldsymbol{m}}{\partial \boldsymbol{x}}\right|_{\boldsymbol{x}=\bar{\boldsymbol{x}},\boldsymbol{u}=\bar{\boldsymbol{u}}} \tag{12}$$

$$[\boldsymbol{R}]_{\boldsymbol{x}} \equiv \left.\frac{\partial \boldsymbol{m}}{\partial \boldsymbol{u}}\right|_{\boldsymbol{x}=\bar{\boldsymbol{x}},\boldsymbol{u}=\bar{\boldsymbol{u}}} \tag{13}$$

And $[\boldsymbol{F}]_{\boldsymbol{Q}}$, $[\boldsymbol{F}]_{\boldsymbol{R}}$, and $[\boldsymbol{F}]_{\boldsymbol{x}}$ are derivatives of f with respect to state, forces, and moments, respectively, which are easily derived. The matrices of partial derivatives with respect to state and control input are what must be determined from the truth model, in this case, numerical lifting-line. Once these matrices have been computed, the covariance of forces and moments due to the known covariance of state and control input can be determined using:

$$[\boldsymbol{P}]_{\boldsymbol{ff}} = [\boldsymbol{Q}]_{\boldsymbol{x}}[\boldsymbol{P}]_{\boldsymbol{xx}}[\boldsymbol{Q}]_{\boldsymbol{x}}{}^{T} + [\boldsymbol{Q}]_{\boldsymbol{u}}[\boldsymbol{P}]_{\boldsymbol{uu}}[\boldsymbol{Q}]_{\boldsymbol{u}}{}^{T} \tag{14}$$

$$[\boldsymbol{P}]_{\boldsymbol{mm}} = [\boldsymbol{R}]_{\boldsymbol{x}}[\boldsymbol{P}]_{\boldsymbol{xx}}[\boldsymbol{R}]_{\boldsymbol{x}}{}^{T} + [\boldsymbol{R}]_{\boldsymbol{u}}[\boldsymbol{P}]_{\boldsymbol{uu}}[\boldsymbol{R}]_{\boldsymbol{u}}{}^{T} \tag{15}$$

Where $[\boldsymbol{P}]_{\boldsymbol{xx}}$ and $[\boldsymbol{P}]_{\boldsymbol{uu}}$ are the covariance matrices of state and control input, respectively. Once these are determined, the covariance matrices for the state update and then the state at the next time step can be determined. In this study, we limit our scope to determining force and moment variances from state and control variances.

III. Numerical Lifting-Line

We present here the basis of numerical lifting-line theory (see [10] for a full derivation). Numerical lifting-line theory models the flow around a given set of lifting surfaces using a distribution of horseshoe vortex filaments, as shown in Fig. 1. The strength of each vortex is specified such that the section lift generated by each vortex as predicted by the vortex lifting law is the same as that predicted by the airfoil section parameters, taking induced downwash from all other vortices into account. This relation is expressed by:

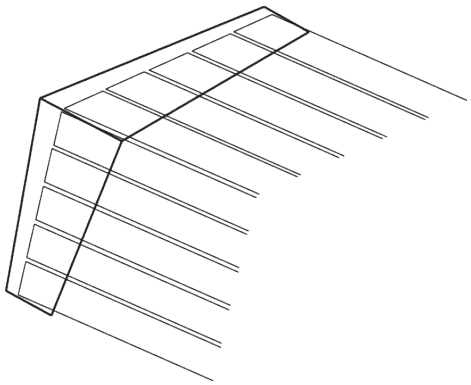

Fig. 1 Distribution of horseshoe vortex filaments along the quarter-chord of a swept wing [14].

$$2\left|\left(\boldsymbol{u}_\infty + \sum_{j=1}^{N} G_j \boldsymbol{v_{ji}}\right) \times \boldsymbol{\zeta_i}\right| G_i - \widetilde{C}_{Li}(\alpha_i, \delta_i) = 0 \tag{16}$$

Where:

$$\boldsymbol{u}_\infty \equiv \frac{\boldsymbol{V}_\infty}{V_\infty} \tag{17}$$

$$\boldsymbol{\zeta_i} \equiv c_i \frac{\boldsymbol{dl_i}}{dS_i} \tag{18}$$

$$G_i \equiv \frac{\Gamma_i}{c_i V_\infty} \tag{19}$$

$$\alpha_i = \arctan\left(\frac{\left(\boldsymbol{u}_\infty + \sum_{j=1}^{N} G_j \boldsymbol{v_{ji}}\right) \cdot \boldsymbol{u_{ni}}}{\left(\boldsymbol{u}_\infty + \sum_{j=1}^{N} G_j \boldsymbol{v_{ji}}\right) \cdot \boldsymbol{u_{ai}}}\right) \tag{20}$$

$$\boldsymbol{v_{ji}} = \begin{cases} \frac{\bar{c}_j}{4\pi}\left(-\frac{\boldsymbol{u}_\infty \times \boldsymbol{r_{j_0 i}}}{r_{j_0 i}(r_{j_0 i} - \boldsymbol{u}_\infty \cdot \boldsymbol{r_{j_0 i}})} + \frac{(r_{j_0 i} + r_{j_1 i})(\boldsymbol{r_{j_0 i}} \times \boldsymbol{r_{j_1 i}})}{r_{j_0 i} r_{j_1 i}(r_{j_0 i} r_{j_1 i} + \boldsymbol{r_{j_0 i}} \cdot \boldsymbol{r_{j_1 i}})} + \frac{\boldsymbol{u}_\infty \times \boldsymbol{r_{j_1 i}}}{r_{j_1 i}(r_{j_1 i} - \boldsymbol{u}_\infty \cdot \boldsymbol{r_{j_1 i}})}\right), & j \neq i \\ \frac{\bar{c}_j}{4\pi}\left(-\frac{\boldsymbol{u}_\infty \times \boldsymbol{r_{j_0 i}}}{r_{j_0 i}(r_{j_0 i} - \boldsymbol{u}_\infty \cdot \boldsymbol{r_{j_0 i}})} + \frac{\boldsymbol{u}_\infty \times \boldsymbol{r_{j_1 i}}}{r_{j_1 i}(r_{j_1 i} - \boldsymbol{u}_\infty \cdot \boldsymbol{r_{j_1 i}})}\right), & j = i \end{cases} \tag{21}$$

Equation (16) is non-linear and must be solved iteratively using Newton's method. Phillips [15] suggests using a linearized version of eq. (16) to obtain an initial guess for the vorticity distribution and then iteratively applying Newton's corrector formula using the Jacobian of eq. (16) to drive the residuals to zero. Once solved, the total aerodynamic force and moment vectors are given by:

$$\boldsymbol{f} = \rho \sum_{i=1}^{N} \Gamma_i \left(\boldsymbol{V}_\infty + \sum_{j=1}^{N} \frac{\Gamma_j \boldsymbol{v_{ji}}}{c_j}\right) \times \boldsymbol{dl_i} \tag{22}$$

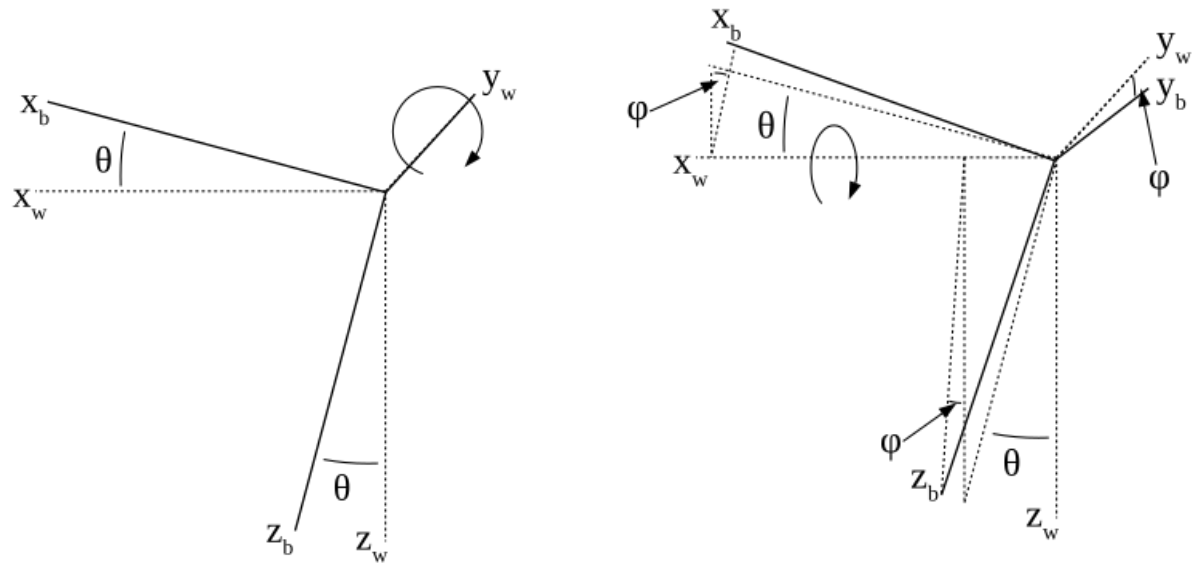

Fig. 2 A perturbation in pitch and a subsequent perturbation in roll with respect to the wind frame.

And:

$$\boldsymbol{m} = \rho \sum_{i=1}^{N} \left[\boldsymbol{r_i} \times \left[\Gamma_i \left(\boldsymbol{V_\infty} + \sum_{j=1}^{N} \frac{\Gamma_j \boldsymbol{v_{ji}}}{c_j} \right) \times \boldsymbol{dl_i} \right] - \frac{1}{2} V_\infty^2 \widetilde{C}_{mi} \int_{s=s_0}^{s_1} c^2 ds \boldsymbol{u_{si}} \right] \tag{23}$$

Where:

$$\boldsymbol{u_{si}} = \boldsymbol{u_{ai}} \times \boldsymbol{u_{ni}} \tag{24}$$

Numerical lifting-line does not include viscous effects. However, viscous effects can be accounted for by integrating airfoil section parameters across each lifting surface using the angle of attack determined by eq. (20).

One limitation of numerical lifting-line is the algorithm fails to grid resolve when there is sideslip on any lifting surface, i.e. the lifting surface is not perpendicular to the freestream [14]. To model vehicle dynamics using numerical lifting-line in this investigation, we limit our investigation to situations where all lifting surfaces remain perpendicular to the freestream. This is satisfied for horizontal lifting surfaces with zero sweep and dihedral in steady, level flight. The vertical stabilizer is rarely perpendicular to the freestream, but this does not cause grid resolution issues if the vertical stabilizer does not generate lift.

Within the scope of this research, two angular perturbations do not introduce spanwise velocity when applied with respect to the wind frame. As shown in Fig. 2, a perturbation in elevation angle about the wind y-axis, here denoted as θ, has no effect on the body y-axis, with which horizontal lifting surfaces are aligned. A subsequent perturbation in bank angle about the wind x-axis, here denoted as ϕ, does shift the body y-axis by ϕ but this axis remains perpendicular to the wind x-axis (see Fig. 2).

The observant reader will note that a roll about the wind x-axis does nothing to change the aerodynamic angles, α and β, and so should have no effect on the aerodynamic forces expressed in the body frame. However, in the context of this investigation, the freestream seen by the tailing aircraft is no longer uniform due to the leading aircraft. This means the aerodynamic forces and moments acting on the tailing aircraft will change as a result of a rotation about the wind x-axis and should be investigated.

IV. Methods

A. Implementation of Numerical Lifting-Line

For this investigation, we use an implementation of numerical lifting-line provided by the Utah State University AeroLab called MachUp [16]. MachUp is written in Fortran with a Python wrapper for interface. MachUp uses the method described above to solve eq. (16) for the distribution of vortex strengths and integrates these according to eqs. (22,23) to find the forces and moments generated by each lifting surface. MachUp also computes viscous effects according to the method described above and includes these in the final solution. Time constraints required using an existing implementation of numerical lifting-line as opposed to writing a new one. MachUp is widely used by aerodynamicists and its accuracy is well-documented [16].

We begin by modelling two different aircraft in MachUp, representative of aircraft that might be used in an aerial recapture situation. We base the lead aircraft off the Lockheed AC-130 (specifications found in [15]). The US military has already begun testing UAVs launched from the AC-130 and is pushing for development of AC-130-based aerial recapture as well [17–20]. The tail aircraft has characteristics typical of small, high-speed, fixed-wing drones. To avoid grid convergence issues, the tailing aircraft has no vertical stabilizer, similar to the X-47B. The leading aircraft does have a vertical stabilizer; however, grid convergence studies show the solution still grid resolves even with the vertical stabilizer included. The specifications for both aircraft are given in Table 4 in the Appendix. Both aircraft are first trimmed with the tailing aircraft 200 ft behind and 50 ft below the lead aircraft. For this investigation, we define trim as a zero moment vector and a lift force exactly balancing the weight of the aircraft (drag force is assumed to be balanced by the thrust, which we do not model). This trimmed state serves as the reference state, $\bar{\boldsymbol{x}}$.

The nonlinear nature of the numerical lifting-line equation makes it impossible to analytically take derivatives of forces and moments with respect to aircraft state. Instead, a central difference approximation provides accuracy sufficient for this application. The Python wrapper computes central difference derivatives for the tailing aircraft at the reference state using:

$$\left.\frac{\partial \boldsymbol{f}}{\partial \boldsymbol{x}}\right|_{\boldsymbol{x}=\bar{\boldsymbol{x}},\boldsymbol{u}=\bar{\boldsymbol{u}}} = \frac{\boldsymbol{f}(\bar{\boldsymbol{x}}+\boldsymbol{dx},\bar{\boldsymbol{u}}) - \boldsymbol{f}(\bar{\boldsymbol{x}}-\boldsymbol{dx},\bar{\boldsymbol{u}})}{2\boldsymbol{dx}} \tag{25}$$

To ensure the lifting-line solutions grid resolve for our modelled situation, we slightly perturb the tailing aircraft in

each degree of freedom, and determine the forces and moments as a function of the number of control points at each perturbed state. We also analyze the value of each aerodynamic derivative as the number of grid points is increased to ensure the solution still grid resolves.

MachUp outputs all forces and moments in the wind frame. The Python wrapper subsequently transforms these to the body frame before computing finite differences, using:

$$\boldsymbol{f_b} = \begin{bmatrix} C_\theta & S_\theta S_\phi & -S_\theta C_\phi \\ 0 & C_\phi & S_\phi \\ S_\theta & -C_\theta S_\phi & C_\theta C_\phi \end{bmatrix} \boldsymbol{f_w} \tag{26}$$

Where C indicates the cosine of the subscripted angle and S indicates the sine. The equations for vehicle dynamics are most easily formulated in the body frame and so it is most useful to have forces and moments expressed in the body frame. However, the perturbations in position and orientation are still defined in a local level, in this case, the wind frame. This most accurately represents how these measurements would be treated by an onboard flight computer.

B. Linear Covariance Analysis

Using the implementation described earlier, we determine the force and moment sensitivity matrices, $[\boldsymbol{Q}]_{\boldsymbol{x}}$, $[\boldsymbol{Q}]_{\boldsymbol{u}}$, $[\boldsymbol{R}]_{\boldsymbol{x}}$, and $[\boldsymbol{R}]_{\boldsymbol{u}}$. We then specify covariance matrices for the state and control inputs. These covariances are typical of UAV state and control uncertainties found in the literature [21–24]. For the purpose of this investigation, the input states and controls are assumed to be uncorrelated and so the covariance matrices, $[\boldsymbol{P}]_{\boldsymbol{xx}}$ and $[\boldsymbol{P}]_{\boldsymbol{uu}}$, have zero off-diagonal terms. Table 1 gives the diagonal elements. As discussed earlier, perturbations in yaw are not considered here. Perturbations in rudder deflection are also not included as the tailing aircraft has no vertical stabilizer. We also choose to not investigate perturbations in velocity and angular rates for the scope of this study.

Table 1 Variance for each degree of freedom of the tailing aircraft.

DOF	Variance	Units
x	9.0	ft^2
y	9.0	ft^2
z	36.0	ft^2
ϕ	9.0	$^{\circ 2}$
θ	9.0	$^{\circ 2}$
δ_a	9.0	$^{\circ 2}$
δ_e	9.0	$^{\circ 2}$

C. Monte Carlo Simulation

We implement a simple Monte Carlo simulation using the model created in MachUp. For each simulation run, a set of normally distributed perturbations in each degree of freedom is generated from the given variances. The tailing aircraft is perturbed accordingly and the forces and moments extracted. The covariances of the force and moment vectors are then determined using:

$$[\boldsymbol{P}]_{ff} \equiv \frac{1}{M-1}\sum_{i=1}^{M}(\boldsymbol{f}-\bar{\boldsymbol{f}})(\boldsymbol{f}-\bar{\boldsymbol{f}})^T \tag{27}$$

$$[\boldsymbol{P}]_{mm} \equiv \frac{1}{M-1}\sum_{i=1}^{M}(\boldsymbol{m}-\bar{\boldsymbol{m}})(\boldsymbol{m}-\bar{\boldsymbol{m}})^T \tag{28}$$

Where $\bar{\boldsymbol{f}}$ and $\bar{\boldsymbol{m}}$ are the force and moment vectors at the reference state.

V. Results

A. Convergence of Lifting-Line Solutions

For all forces and moments, the value converges to within 5% of the final value with a resolution of 316 grid points per lifting surface. Figure 3 shows typical convergence for the force and moment solutions obtained from numerical lifting-line.

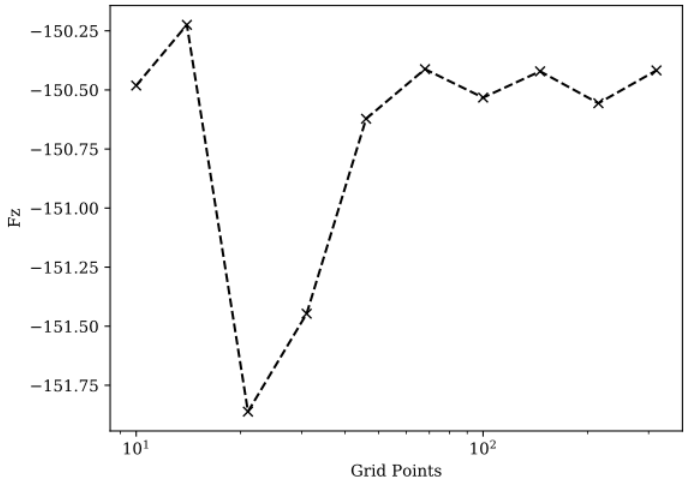

Fig. 3 Grid convergence force [lbf] in the body z-direction on the tailing aircraft after being perturbed one foot forward from the trim state.

For all derivatives, the value converges to within 5% of the final value with a resolution of 316 grid points per lifting surface. Figures 4 and 5 show the best and worst grid convergence of all aerodynamic derivatives computed. All other

derivatives show grid resolution behavior between these two cases. From this study, we determine 100 grid points is an appropriate resolution for all subsequent calculations.

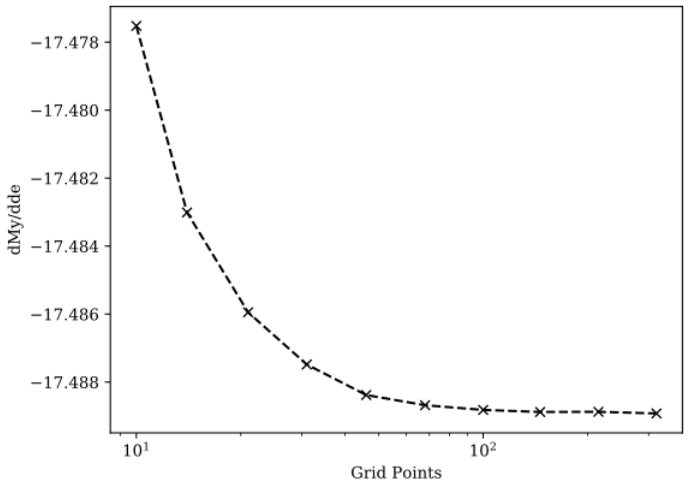

Fig. 4 Grid convergence of $\frac{\partial m_y}{\partial \delta_e}$ $[ft * lbf/^\circ]$.

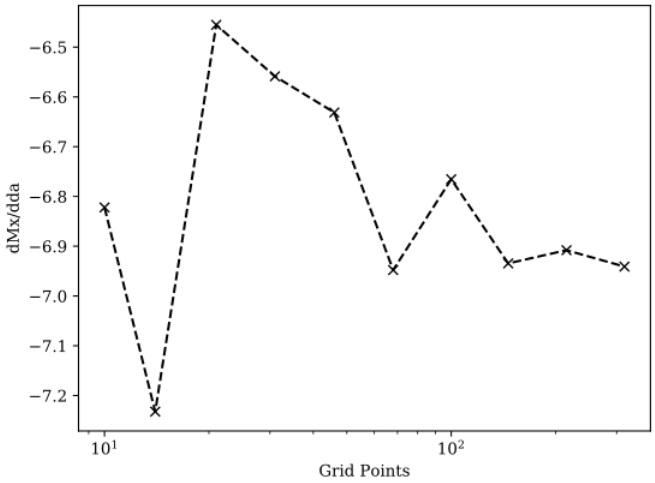

Fig. 5 Grid convergence of $\frac{\partial m_x}{\partial \delta_a}$ $[ft * lbf/^\circ]$.

B. Covariance Propagation

Propagating the state and control variances given in Table 1 through eqs. (14,15) using the derivative matrices acquired from lifting-line, we determine the following force and moment covariances:

$$[P]_{ff} = \begin{bmatrix} 66.673 & 0.0 & -796.732 \\ 0.0 & 0.0 & 0.0 \\ -796.732 & 0.0 & 9525.223 \end{bmatrix} \tag{29}$$

$$[P]_{mm} = \begin{bmatrix} 411.984 & 0.0 & -5.631 \\ 0.0 & 4207.763 & 0.0 \\ -5.631 & 0.0 & 0.078 \end{bmatrix} \tag{30}$$

As expected, linear covariance analysis predicts no coupling between longitudinal and lateral forces and moments. From 1000 Monte Carlo runs, we obtain the following covariances:

$$[P]_{ff} = \begin{bmatrix} 80.800 & 0.003 & -730.306 \\ 0.003 & 0.0 & -0.017 \\ -730.306 & -0.017 & 9447.959 \end{bmatrix} \tag{31}$$

$$[P]_{mm} = \begin{bmatrix} 406.636 & -24.563 & -5.725 \\ -24.563 & 1983.574 & 0.206 \\ -5.725 & 0.206 & 0.117 \end{bmatrix} \tag{32}$$

The results of the Monte Carlo simulation do seem to show some longitudinal-lateral coupling; however, these terms are typically small compared to the other covariances and tend towards zero over multiple runs of the simulation, and so can be neglected. The variances of f_y and m_z are much smaller than other variances. This is because we do not induce any sideslip on the tailing aircraft, which is the typical cause of side force and yawing moments, and so these terms can also be neglected in the present study.

The percent errors between the results predicted by linear covariance and Monte Carlo are:

$$[E]_{ff} = \begin{bmatrix} 17.48\% & 100\% & 9.10\% \\ 100\% & 40.68\% & 100\% \\ 9.10\% & 100\% & 0.82\% \end{bmatrix} \tag{33}$$

$$[\boldsymbol{E}]_{\boldsymbol{mm}} = \begin{bmatrix} 1.32\% & 100\% & 1.65\% \\ 100\% & 1.58\% & 100\% \\ 1.65\% & 100\% & 33.41\% \end{bmatrix} \tag{34}$$

Linear covariance shows agreement with Monte Carlo within 10% for all terms except for $\boldsymbol{f_x}$. To reduce the error in the variance of $\boldsymbol{f_x}$ to below 10%, the input variances must be reduced to those given in Table 2. For these input variances, all significant terms of the covariance matrices predicted by linear covariance analysis agree to within 10% of Monte Carlo simulation.

Table 2 Variance for each degree of freedom of the tailing aircraft such that the variances predicted by linear covariance analysis agree to within 10% of Monte Carlo results.

DOF	Variance	Units
x	9.0	ft^2
y	9.0	ft^2
z	36.0	ft^2
ϕ	9.0	$\circ^2$
θ	1.0	$\circ^2$
δ_a	1.0	$\circ^2$
δ_e	1.0	$\circ^2$

When implemented as part of a full GN&C solution, a controller is included to adjust the throttle of the UAV so as to balance $\boldsymbol{f_x}$. This means large variances in $\boldsymbol{f_x}$ can be ignored, as the controller will quickly act to negate them. If we neglect variances containing $\boldsymbol{f_x}$, a larger range of input variances can be handled by linear covariance while still producing accurate results. The input variances given in Table 3 are the maximum that will give results that agree to within 10% of the results of Monte Carlo.

Table 3 Variance for each degree of freedom of the tailing aircraft such that the variances predicted by linear covariance analysis, except for f_x, agree to within 10% of Monte Carlo results.

DOF	Variance	Units
x	400.0	ft^2
y	400.0	ft^2
z	400.0	ft^2
ϕ	100.0	$\circ^2$
θ	49.0	$\circ^2$
δ_a	100.0	$\circ^2$
δ_e	100.0	$\circ^2$

These results show linear covariance analysis can effectively reproduce the results of Monte Carlo simulation within

a reasonable range of perturbations. When included as part of a full GN&C solution, we expect the accuracy of linear covariance analysis coupled with numerical lifting-line to be even better. Both the Monte Carlo simulations and linear covariance analysis were written to run in parallel, and linear covariance consistently ran approximately 10^2 times faster than Monte Carlo.

C. Note on Design of the Tailing Aircraft

As discussed earlier, the variance in $\boldsymbol{f_x}$ typically limits the range of input covariance to which linear covariance can be applied. An examination of aircraft forces and moments as a function of state reveals the force in the body x-direction is parabolic with respect to multiple aircraft state variables, as shown in Fig. 6. When the reference state of the aircraft exists near the vertex of these parabolas, a linear derivative of the force or moment at that point will hardly reflect the true behavior of the system over a wide range of possible states. When designing an aircraft where linear covariance analysis will be part of the control logic, it may be desirable to design the aircraft so it operates in a region further from these vertices where the behavior is more linear.

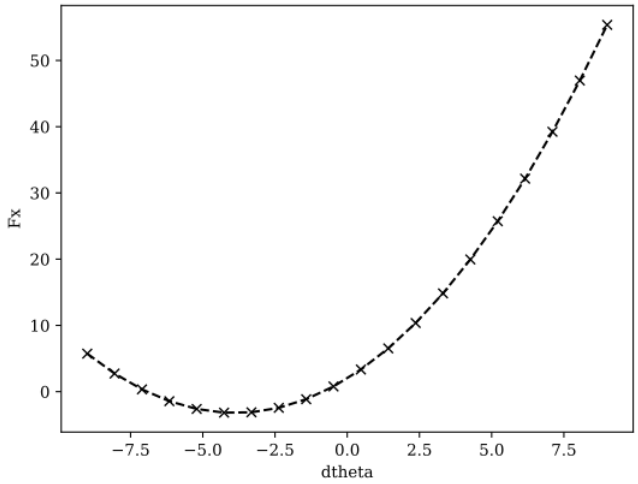

Fig. 6 Force [lbf] in the body x-direction as a function of aircraft elevation angle perturbation.

VI. Future Work

This investigation is limited due to numerical lifting-line not being able to reliably model situations where there is sideslip. Research is currently being conducted at Utah State University to improve numerical lifting-line so that the algorithm grid resolves even when spanwise flow is introduced (Reid, J, private communication). This research is showing promising results and nears completion. Once a solution is found, we will revisit this investigation to determine the effects of yaw and rudder deflection.

Further investigation would also study the effect of including perturbations in the tailing aircraft's relative velocity and angular rate. This would apply linear covariance to the entire state of the aircraft. Once the full state of an aircraft has been considered, this investigation can be expanded to analyze the behavior of a complete GN&C solution coupled to the aerodynamic model. This will show the extent of the effectiveness of linear covariance and numerical lifting-line in analyzing various recapture trajectories. This can also be expanded to other situations, such as unmanned aerial refueling, UAV swarms, and aircraft carrier landing.

VII. Conclusion

We successfully show linear covariance analysis is readily applied to situations where numerical lifting-line theory is used as the vehicle dynamics model, such as the aerial recapture of a UAV. When the variance of the body-x force is neglected, linear covariance analysis produces accurate results up to large values of covariance in position and orientation. These results agree to within 10% of Monte Carlo simulations but with a fraction of the computational cost.

Appendix

Table 4 gives the specifications for the lead and tailing aircraft modelled in this investigation.

Table 4 Specifications for the lead and tail aircraft. For the lead aircraft, the main wing has a NACA 2410 section and the horizontal and vertical stabilizers have a NACA 0010 section. For the tailing aircraft, all lifting surfaces have a NACA 0010 section.

Specification	Lead Aircraft	Tail Aircraft	Units
W	155000	150	lbf
S_w	1745	7.5	ft^2
b_w	132.6	6.0	ft
R_{T_w}	0.57	1.0	-
Λ_w	0.0	0.0	$^\circ$
α_{0w}	0.0	1.63	$^\circ$
x_w	2.5	0.0	ft
y_w	0.0	0.0	ft
z_w	-7.4	0.0	ft
S_h	528	2.0	ft^2
b_h	52.7	2.0	ft
R_{T_h}	0.35	1.0	-
Λ_h	0.0	0.0	$^\circ$
α_{0h}	-1.5	0.0	$^\circ$
x_h	-44.5	-8.0	ft
y_h	0.0	0.0	ft
z_h	-7.4	0.2	ft
S_v	253	0.8	ft^2
b_v	22	1.0	ft
R_{T_v}	0.278	1.0	-
Λ_v	0.0	-	$^\circ$
α_{0v}	0.0	-	$^\circ$
x_v	-42	-	ft
y_v	0.0	-	ft
z_v	-7.4	-	ft

Funding Sources

Funding for this research was provided by the Air Force Research Laboratory Summer Faculty Fellowship Program 2019.

Acknowledgments

Special thanks is given to Dr. Doug Hunsaker and the USU AeroLab for providing MachUp. Special thanks is also given to Josh Goates for his invaluable input. We also express gratitude to Dr. Rob Leishman and the AFIT ANT Center for their support and welcome.

References

[1] Christensen, R. S., and Geller, D., "Linear Covariance Techniques for Closed-Loop Guidance Navigation and Control System Design and Analysis," *Proceedings of the Institute of Mechanical Engineers Part G: Journal of Mechanical Engineering*, 2012, pp. 44–65.

[2] Geller, D. K., and Christensen, D. P., "Linear Covariance Analysis for Powered Lunar Descent and Landing," *Journal of Spacecraft and Rockets*, Vol. 46, No. 6, 2009.

[3] Arneberg, J. T., "Guidance Laws for Partially-Observable UAV Interception Based on Linear Covariance Analysis," Master's thesis, Massachusetts Institute of Technology, June 2018.

[4] Arneberg, J., Tal, E., and Karaman, S., "Guidance Laws for Partially-Observable Interception Based on Linear Covariance Analysis," *2018 IEEE/RSJ International Conference on Intelligent Robots and Systems (IROS)*, 2018.

[5] Moesser, T. J., "Guidance and navigation linear covariance analysis for lunar powered descent," Master's thesis, Utah State University, 07 2010.

[6] Christensen, R. S., and Geller, D., "Closed-Loop Linear Covariance Analysis for Hosted Payloads," *Journal of Guidance, Control & Dynamics*, Vol. 41, No. 10, 2018.

[7] Ma, Y., Liu, H., Zhang, Y., He, Q., and Xu, Z., "Monte Carlo approach to the analysis of UAVs control system." *Proceedings of 2014 IEEE Chinese Guidance, Navigation and Control Conference*, 2014, p. 458.

[8] Masri, M. A., Dbeis, S., and Al Saba, M., "Autolanding a Power-off UAV Using On-line Optimization and Slip Maneuvers." *Journal of Intelligent and Robotic Systems*, Vol. 86, No. 2, 2017, p. 255.

[9] Ma, Y., Liu, H., Zhang, Y., He, Q., and Xu, Z., "Intelligent decision making for UAV based on Monte Carlo Simulation," *2018 15th International Conference on Control, Automation, Robotics and Vision (ICARCV)*, 2018, pp. 521–525.

[10] Phillips, W. F., and Snyder, D. O., "Modern Adaptation of Prandtl's Classic Lifting-Line Theory," *Journal of Aircraft*, Vol. 37, No. 4, 2000.

[11] Spall, R. E., Phillips, W. F., and Pincock, B. B., "Numerical analysis of multiple, thin-sail geometries based on Prandtl's lifting-line theory," *Computers and Fluids*, Vol. 82, No. 15, 2013.

[12] Sprinkle, J., Eklund, J. M., and Sastry, S. S., "Deciding to land a UAV safely in real time," *Proceedings of the 2005, American Control Conference, 2005*, IEEE, 2005, pp. 3506 – 3511 vol. 5.

[13] Gelb, A., *Applied Optimal Estimation*, 1st ed., The MIT Press, Cambridge, Massachusetts, 1974, Chaps. 3.6-7, pp. 72–78.

[14] Hunsaker, D., "A Numerical Lifting-Line Method Using Horseshoe Vortex Sheets," *Rocky Mountain Space Grant Consortium Meeting Proceedings*, 2011, pp. 1–11.

[15] Phillips, W. F., *Mechanics of Flight*, 2nd ed., John Wiley & Sons, Hoboken, New Jersey, 2010, Chap. 1.9, pp. 94–107.

[16] Hunsaker, D. F., "USU AeroLab," , 2018. `aero.go.usu.edu`.

[17] Harper, J., "Special Operations Gunships to Be Equipped With Improved Sensors," *National Defense*, 2016.

[18] Harper, J., "Gunship-Launched Drone Approaches Transition Point," *National Defense*, 2017.

[19] Vision, U., "US Air Force Research Lab to Extend Aircraft ISR Range," *UAS Vision*, 2017.

[20] Howard, B., "DARPA's 'Gremlin' Drones Can Deploy From A Flying Carrier In Starcraft-Style Swarms," *Task & Purpose*, 2018.

[21] Cortes, C., Shahbazi, M., and Menard, P., "UAV-LiCAM System Development: Calibration and Geo-Referencing," *ISPRS - International Archives of the Photogrammetry, Remote Sensing and Spatial Information Sciences*, Vol. XLII-1, 2018, pp. 107–114.

[22] Laupre, G., Khaghani, M., and Skaloud, J., "Sensitivity to Time Delays in VDM-Based Navigation," *Drones*, Vol. 3, No. 11, 2019.

[23] Shults, R., "Simulation of Inertial Navigation System Errors at Aerial Photography from UAV," *ISPRS - International Archives of the Photogrammetry, Remote Sensing and Spatial Information Sciences*, Vol. XLII-1/W1, 2017, pp. 345–351.

[24] Khaghani, M., and Skaloud, J., "Application of Vehicle Dynaic Modeling in UAVs for Precise Determination of Exterior Orientation," *ISPRS - International Archives of the Photogrammetry, Remote Sensing and Spatial Information Sciences*, Vol. XLI-B3, 2016, pp. 827–831.